

NICKEL-BASE MATERIAL SOLUTIONS TO METAL DUSTING PROBLEMS

B. A. Baker, G. D. Smith, V. W. Hartmann, L. E. Shoemaker
Special Metals Corporation
3200 Riverside Drive
Huntington, WV

S. A. McCoy
Special Metals Wiggin, Ltd.
Holmer Road, UK

ABSTRACT

Long-term testing has been conducted in a laboratory environment which promotes metal dusting. The results have confirmed the desirability of a nickel alloy matrix as well as certain alloying additions which promote formation of a protective oxide scale to prevent carbon ingress. A new Ni-Cr-Fe-Al alloy has been shown to exhibit the greatest overall resistance to metal dusting, as confirmed by over 15,000 hours of testing in the laboratory in addition to several thousand hours of in-situ testing in syngas environments. General corrosion, mechanical and physical properties and weldability results for this new alloy are discussed.

INTRODUCTION

Metal dusting can be described as a catastrophic form of carburization occurring under conditions where the carbon activity of the gaseous atmosphere is greater than one. The phenomenon can produce rapid metal wastage, producing pits and grooves as the affected metal disintegrates into a mixture of powdery carbon and metal particles. Metal dusting corrosion has negatively impacted the efficiency and productivity of processes within numerous industries. These include petrochemical processing (processes involving steam reforming of methane or natural gas, such as ammonia and methanol production), direct iron-ore reduction and heat treating.

Considerable focus has been placed upon improvement of reforming technologies. Reduction in the ratio of steam to hydrocarbon feed stock has been employed in many cases in order to increase process efficiency. However, this action also increases carbon activity of the syngas produced. This in turn increases the propensity for metal dusting attack to occur. Efforts to improve catalyst efficiency have led to the use of nickel oxide catalysts which have no tolerance for sulfur in the system. Sulfur-containing species such as H_2S have in the past been used to 'poison' metal surfaces and minimize the occurrence of metal dusting, and while this effect has been confirmed both in the laboratory¹ and in the field, the utility of this method as a means of control is now quite limited. Avoidance of the metal dusting temperature regime in syngas environments (roughly 450°C to 800°C) has typically been achieved by rapidly quenching the syngas from the production temperature greater than 800°C to less

than 450°C along a short transfer line before it enters a boiler. However, the desire to achieve higher levels of efficiency and productivity has produced new processes which involve exposure of entire units constructed of metallic components to metal dusting conditions. Such aggressive design requires materials which are capable of withstanding extremely aggressive conditions for long periods. Such performance requires an alloy which is capable of forming and sustaining an adherent, protective and healable oxide layer.

EXPERIMENTAL

Table 1 shows the chemical composition for each alloy discussed in this paper. Corrosion test specimens were ground to a 120-grit finish for standardization purposes. Metal dusting samples measured approximately 2.5cm X 2.5cm X thickness. Oxidation and carburization test samples were in the form of cylindrical pins, measuring 11.8mm in diameter and 19.1mm in length. Samples were exposed in sealed horizontal electrically-heated furnaces having mullite tubes. A sealed push-rod type mechanism was used for sample insertion and removal. Metal dusting test samples were cycled, lightly brushed, ultrasonically cleaned in methanol and weighed at two-week intervals. In addition to mass change, pitting depth was also determined for each sample using an optical microscope having a calibrated fine focus knob. Oxidation and carburization test samples were cycled and weighed at one-week intervals.

METAL DUSTING RESULTS

Mass loss rate as a function of time is shown in Figure 1. Figure 2 shows the result of multiple regression analysis of the log of the mass loss rate, calculated by averaging the mass loss rate over the total testing duration, versus a summation of the weight percentage of various alloying additions. The summation coefficients were based upon the regression results. Only the austenitic nickel-base alloys and Fe-Ni-Cr alloys were included in this calculation; the mechanically alloyed ferritic alloy, 956, and also alloy 400 were excluded. The best fit ($r^2=0.92$) was obtained using the following summation versus the log of the mass loss rate:

$$(\text{Ni}\% + \text{Co}\%) + 72.4\text{Si}\% + 43.4\text{Al}\% + 41.3\text{Ti}\% + 10.2\text{Cr}\% + 6.2(\text{Mo}\% + \text{W}\%) - 1.3\text{Fe}\%.$$

For comparison, a similar plot was created using Schillmoller's empirical chromium equivalent equation² which correlates metal dusting resistance with the following summation:

$$\text{Cr}_{\text{equiv.}} = \text{Cr}\% + 3(\text{Si}\% + \text{Al}\%).$$

Figure 3 shows the log of the pit progression rate versus the $\text{Cr}_{\text{equiv.}}$ summation ($r^2=0.62$).

The maximum pit depth as a function of time is plotted in Figure 4. Table 2 shows the pit progression rate for each alloy tested. The same regression technique used for the mass loss rate was used to characterize the variation in the log of the pitting depth with a summation of certain alloying additions. Again, only the austenitic nickel-base and Fe-Ni-Cr alloys were included in the calculation. The best fit ($r^2=0.89$) was produced using the following summation (multiples of weight percentage) versus the log of the pit progression rate (Figure 5):

$$(\text{Ni}\% + \text{Co}\%) + 30.9\text{Ti}\% + 30\text{Al}\% + 23.7\text{Si}\% + 4.8(\text{Mo}\% + \text{W}\%) + 3\text{Cr}\% - 1.9\text{Fe}\%.$$

The Schillmoller chromium equivalent was also correlated with the log of the mass loss rate for comparison, as shown in Figure 6 ($r^2=0.38$).

While it is apparent that carbide-forming elements such as Mo, W and Ti can enhance performance in nickel-base alloys with chromium levels significantly lower than 25% (e.g. alloys 625, 263, and 617), reliance upon a sustainable and healable oxide is preferred for long-term performance. Based upon observed pitting rates and mass loss rates in laboratory testing, and the results of in situ field exposures, alloy 693 offers the most promising performance to end users seeking metal dusting-resistant materials. Figure 7 shows a photomicrograph of a cross section from an alloy 693 sample exposed for 15,816 hours at 621°C in CO-20% H₂, showing the thin, adherent surface oxide.

ALLOY 693 PROPERTIES

Mechanical Properties

While corrosion resistance is of utmost importance in applications which may cause metal dusting, mechanical properties are also an important consideration when selecting a material. The following data are intended to highlight the properties of the newly-introduced alloy 693. Table 3 shows room-temperature tensile results for alloy 693 before and after intermediate-temperature exposure. The room-temperature tensile properties for as-produced alloy 693 material are similar to those for alloy 690. Very respectable elongation values are maintained after exposure times of up to 2000 hours in the critical temperature range of 593°C to 760°C. Figure 8 shows the elevated temperature tensile properties of alloy 693 hot-rolled rod in the annealed condition. Table 4 shows long-term stress rupture data for alloy 693 including elongation and reduction of area; Figure 9 compares the stress rupture properties of alloys 601, 617, 690 and 693 via a Larson-Miller plot. At temperatures below about 871°C (1600°F), alloy 693 possesses greater rupture strength than alloy 601. The properties of the alloy 693 at 1800°F are more similar to those expected for alloy 690. Figure 10 shows stress versus rupture life for alloy 693.

Physical Properties

Comparison of thermophysical properties (thermal conductivity, specific heat and coefficient of expansion) versus temperature for alloys 693, 601 and 690 is made in Tables 5 to 7. Table 8 shows values for the melting range of alloy 693 as well as density and electrical resistivity at room temperature.

High Temperature Oxidation and Carburization Resistance

Figures 11 and 12 show mass change results for alloy 693 compared with other high temperature alloys in air plus 5% water vapor at 1000°C (2012°F) and 1200°C (2192°F). Alloy 693, by virtue of its high aluminum content, possesses excellent resistance to oxidation. Alloy 693 also exhibits excellent resistance to high temperature carburization, as evidenced by the data shown in Figure 13, which was obtained by exposure of alloy samples in H₂-5.5% CH₄-4.5% CO₂ at 1000°C (1832°F).

Welding Trials

Table 9 shows room-temperature and 649°C (1200°F) tensile results for similar and dissimilar full-penetration butt welds performed on alloy 693 hot-rolled and annealed plate (20mm thick). All welds were performed using the GTAW process with a 2% thoriated electrode using 100% argon as the shielding gas. The welding wire diameter was 0.093". Transverse 2T side bends were performed for

each weld joint, and all bends were acceptable per ASME code standards. All welds were also examined using X-ray photography with no indications detected. The tested samples for the 693-to-601 welds have been received and evaluated, but the others have not. However, based upon the observed properties, it appears that fracture has occurred in the weld in every sample. Elongation values for samples tested in the transverse orientation, with the weld placed at the center of the sample, are somewhat biased toward the low end of the range due to the fact that elongation of the sample gage section was not uniform and was likely restricted to the weld metal. For the transverse sample, reduction of area represents a much better indication of the material ductility at the point of fracture.

CONCLUSIONS

Alloy 693 offers a combination of properties which make it an attractive choice for resistance to harshly corrosive high temperature environments, particularly those conditions which promote metal dusting. The material has been shown to be readily weldable and to exhibit desirable engineering properties in addition to its excellent corrosion properties.

REFERENCES

1. A. Schneider, et al., *Materials and Corrosion*, 49, 1998, p. 336.
2. S. B. Parks and C. M. Schillmoller, *Stainless Steel World*, 9 (3), 1997, p. 44.

Table 1. Nominal Composition of Commercial Alloys

Alloy	Ni	Cr	Fe	Mn	Si	Al	Ti	C	Other
754	78	20	-	-	-	0.3	0.5	0.05	0.5 Y ₂ O ₃
TD	73	22	-	-	1.4	-	-	0.01	3.0 Mo
600	72	15.5	8	0.3	0.3	0.3	0.3	0.08	-
758	67	30	-	-	-	0.4	0.5	0.05	0.5 Y ₂ O ₃
400	64	0.1	1.6	0.7	0.1	0.02	0.4	0.15	32.2 Cu
693	62	29	4	-	-	3.1	-	-	Nb, Zr
602CA	62	25	9.5	-	-	2.2	-	0.18	Y,Zr
625	61	21.5	2.5	-	0.1	0.2	0.2	0.02	9 Mo, 3.6 Nb
601	60.5	23	13	0.2	0.2	1.4	0.4	0.05	-
690	59	29	9	0.2	0.1	0.3	0.3	0.02	-
C-276	57	15.5	5.5	-	-	0.1	0.2	-	3.8 W
671	53	46	-	-	-	0.3	0.3	0.03	-
617	55	22	1	-	0.1	1.2	0.4	0.08	12.5 Co, 9.7 Mo
263	51	20	39	0.3	0.1	0.5	2.2	0.06	20 Co, 5.9 Mo
825	42	21.5	28	0.4	0.1	0.1	1	0.02	3 Mo, 2Cu
DS	37	16	41	1.0	2.3	-	-	0.08	-
330	35	19	44	1.0	1.3	-	-	0.07	-
803	34	27	36	1.0	0.8	0.4	0.4	0.08	-
864	34	21	39	0.4	0.8	0.3	0.6	0.03	4.2 Mo
800/800HT	32	21	45	0.9	0.1	0.4	0.4	0.07	-
956	-	20	75	-	-	4.5	0.5	0.05	0.5 Y ₂ O ₃

Table 2
Pitting Progression Rate after Exposure in CO-20% H₂ at 621°C

Alloy	Pit Depth		Exposure Time	Pit Progression Rate	Pit Progression Rate
	Mils	mm	Hours	Mils per Hour	mm/h
800	25.0	635	1056	2.37E-02	9.32E-04
330	17.0	432	1056	1.61E-02	6.34E-04
DS	24.0	610	2400	1.00E-02	3.94E-04
803	21.5	546	2400	8.96E-03	3.53E-04
825	7.0	178	1662	4.21E-03	1.66E-04
864	9.1	231	2184	4.17E-03	1.64E-04
601	19.8	503	6600	3.00E-03	1.18E-04
602CA	15.0	381	10776	1.39E-03	5.48E-05
600	1.8	46	1392	1.29E-03	5.09E-05
956	18.6	472	15936	1.17E-03	4.60E-05
754	3.3	84	2936	1.12E-03	4.43E-05
TD	7.3	185	6728	1.09E-03	4.27E-05
263	17.0	432	15936	1.07E-03	4.20E-05
625	6.3	160	6397	9.85E-04	3.88E-05
758	7.0	178	8023	8.72E-04	3.44E-05
690	12.1	307	14160	8.55E-04	3.36E-05
C-276	4.0	102	6397	6.25E-04	2.46E-05
671	3.6	91	9016	3.99E-04	1.57E-05
617	1.6	41	14160	1.13E-04	4.45E-06
693	1.7	43	15816	1.07E-04	4.23E-06

Table 3
Room-Temperature Tensile Results for Alloy 693

Exposure Temperature, °C (°F)	Exposure Time, Hours	0.2% Yield Strength, MPa (ksi)	Ultimate Tensile Strength, MPa (ksi)	Elongation, %
As-Produced	As-Produced*	410 (59.5)	834 (121.0)	43.0
593 (1100)	1000	745 (108)	1145 (166)	31
649 (1200)	500	827 (120)	1207 (175)	29
649 (1200)	1000	827 (120)	1214 (176)	28
649 (1200)	2000	703 (102)	1110(161)	31
704 (1300)	500	827 (120)	1186 (172)	27
704 (1300)	1000	807 (117)	1179 (171)	31
760 (1400)	500	703 (102)	1103 (160)	32
760 (1400)	1000	717 (104)	1117 (162)	31
760 (1400)	2000	552 (80)	1020 (148)	31

* Hot-Rolled and Annealed Rod

Table 4
Stress Rupture Data Points for Alloy 693 Showing Elongation and Reduction of Area

Temperature, °C (°F)	Stress, MPa (ksi)	Rupture Life, h	Elongation, %	Reduction of Area, %
649 (1200)	221 (32)	1704	9	14.8
704 (1300)	138 (20)	1512	14.4	12.6
760 (1400)	90 (13)	1716	10.2	23.8
816 (1500)	62 (9)	687	43	33.8
871 (1600)	41 (6)	1021	26	21.8
982 (1800)	10 (1.5)	2071	100.5	n/a

Table 5
Thermal Conductivity for Alloys 693, 601 and 690

Temperature, °F	Thermal Conductivity		
	Btu-in./ft ² -h-°F		
	Alloy 693	Alloy 601	Alloy 690
RT	64	78	n/a
200	73	87	93
400	89	100	107
600	103	113	122
800	117	126	136
1000	131	139	151
1200	143	153	165
1400	155	165	179
1600	165	178	194
1800	176	190	207
2000	186	203	n/a
2100	192	N/a	n/a
Temperature, °C	W/m-°C		
	Alloy 693	Alloy 601	Alloy 690
	RT	9.1	11.2
100	10.7	12.7	13.5
200	12.6	14.3	15.4
300	14.2	16.0	17.3
400	16.1	17.7	19.1
500	17.8	19.5	21.0
600	19.5	21.0	22.9
700	21.6	22.8	24.8
800	22.8	24.4	26.6
900	23.6	26.1	28.5
1000	25.2	27.8	30.1
1100	26.8	N/a	n/a
1150	27.5	N/a	n/a

Table 6
Specific Heat Values for Alloys 693, 601 and 690

Temperature °F	Specific Heat		
	Btu/lb-°F		
	Alloy 693	Alloy 601	Alloy 690
RT	0.109	0.107	0.107
200	0.115	0.112	0.112
400	0.121	0.119	0.119
600	0.127	0.126	0.126
800	0.131	0.133	0.133
1000	0.135	0.14	0.14
1200	0.14	0.147	0.148
1400	0.145	0.155	0.155
1600	0.151	0.162	0.162
1800	0.156	0.169	0.169
2000	0.159	0.176	0.176
Temperature °C	J/kg-°C		
	Alloy 693	Alloy 601	Alloy 690
RT	455	448	450
100	484	469	471
200	505	498	497
300	525	523	525
400	548	548	551
500	560	578	578
600	579	603	604
700	598	632	631
800	616	657	658
900	642	686	684
1000	662	712	711

Table 7
Coefficient of Expansion for Alloy 693, Alloy 601 and Alloy 690

Temperature °F	Coefficient of Expansion ^a		
	10 ⁻⁶ in./in./°F		
	Alloy 693	Alloy 601	Alloy 690
200	7.22	7.6	7.8
400	7.57	8.01	7.97
600	7.84	8.11	8.11
800	8.09	8.3	8.29
1000	8.28	8.5	8.53
1200	8.6	8.87	8.87
1400	9.02	9.19	9.14
1600	9.38	9.51	9.38
Temperature °C	mm/m/°C		
	Alloy 693	Alloy 601	Alloy 690
	100	13.04	13.75
200	13.61	14.36	14.31
300	14.05	14.58	14.53
400	14.42	14.83	14.80
500	14.80	15.19	15.19
600	15.22	15.62	15.70
700	15.72	16.11	16.18
800	16.32	16.67	16.60
900	17.01*	17.24	17.01*

^aMean coefficient of linear expansion between 78°F (26°C) and temperature shown.

Table 8
Physical Constants for Alloy 693

Density, g/cm ³	7.63
lb/in. ³	0.275
Melting Range, °C	1317-1367
°F	2403-2493
Electrical Resistivity at 24°C (75°F), Ω-circ mil/ft	702.7
μΩ-m	1.168

Table 9
Room-Temperature and Elevated-Temperature Tensile Results for Similar and Dissimilar Alloy
693 Welds (0.8" Hot-Rolled and Annealed Plate) Performed using GTAW

Temperature °C (°F)	0.2% Yield Strength MPa (ksi)	Tensile Strength MPa (ksi)	Elongation %	Reduction Of Area, %	Base Metal(s)	Filler Metal	Orientation	Breakage Location
20 (68)	448 (65)	648 (94)	20.4	38.6	693	52	Transverse	n/a
20 (68)	538 (78)	696 (101)	31.4	56	693	52	Transverse	n/a
649 (1200)	338 (49)	448 (65)	23	58.8	693	52	Transverse	n/a
649 (1200)	324 (47)	441 (64)	27.6	53.2	693	52	Transverse	n/a
649 (1200)	324 (47)	441 (64)	24	54.6	693	52	AWM*	---
649 (1200)	359 (52)	469 (68)	26.2	44	693	52	AWM*	---
20 (68)	531 (77)	669 (97)	24.4	64.4	693/800	82	Transverse	n/a
20 (68)	483 (70)	669 (97)	25.2	65.8	693/800	82	Transverse	n/a
649 (1200)	365 (53)	524 (76)	22.8	46.4	693/800	82	Transverse	n/a
649 (1200)	359 (52)	524 (76)	26.2	48.4	693/800	82	Transverse	n/a
20 (68)	469 (68)	731 (106)	29.8	46.8	693/600	82	Transverse	n/a
20 (68)	462 (67)	669 (97)	28	54	693/600	82	Transverse	n/a
649 (1200)	351 (51)	510 (74)	25.8	42.6	693/600	82	Transverse	n/a
649 (1200)	359 (52)	524 (76)	32.2	57	693/600	82	Transverse	n/a
20 (68)	455 (66)	565 (82)	13.0	29.0	693/601	601	Transverse	Weld
20 (68)	414 (60)	621 (90)	32.8	47.6	693/601	601	Transverse	Weld
20 (68)	407 (59)	634 (92)	39.0	56.4	693/601	601	AWM*	---
20 (68)	393 (57)	614 (89)	32.0	48.8	693/601	601	AWM*	---
649 (1200)	345 (50)	434 (63)	11.4	32.2	693/601	601	Transverse	Weld
649 (1200)	331 (48)	469 (68)	21.8	36.4	693/601	601	Transverse	Weld
649 (1200)	372 (54)	510 (74)	19.4	47.0	693/601	601	AWM*	---
649 (1200)	345 (50)	469 (68)	28.2	35.4	693/601	601	AWM*	---

* - All Weld Metal.

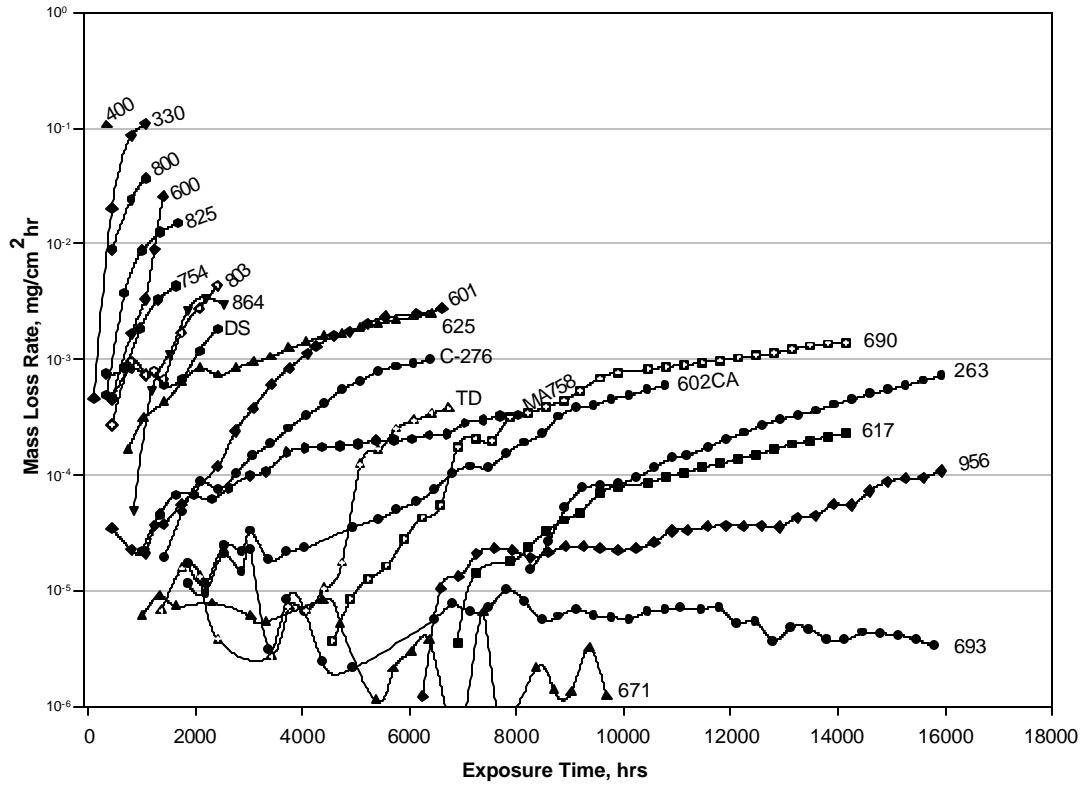


Figure 1. Mass loss rate versus exposure time for alloy samples exposed to CO-20% H₂ at 621°C.

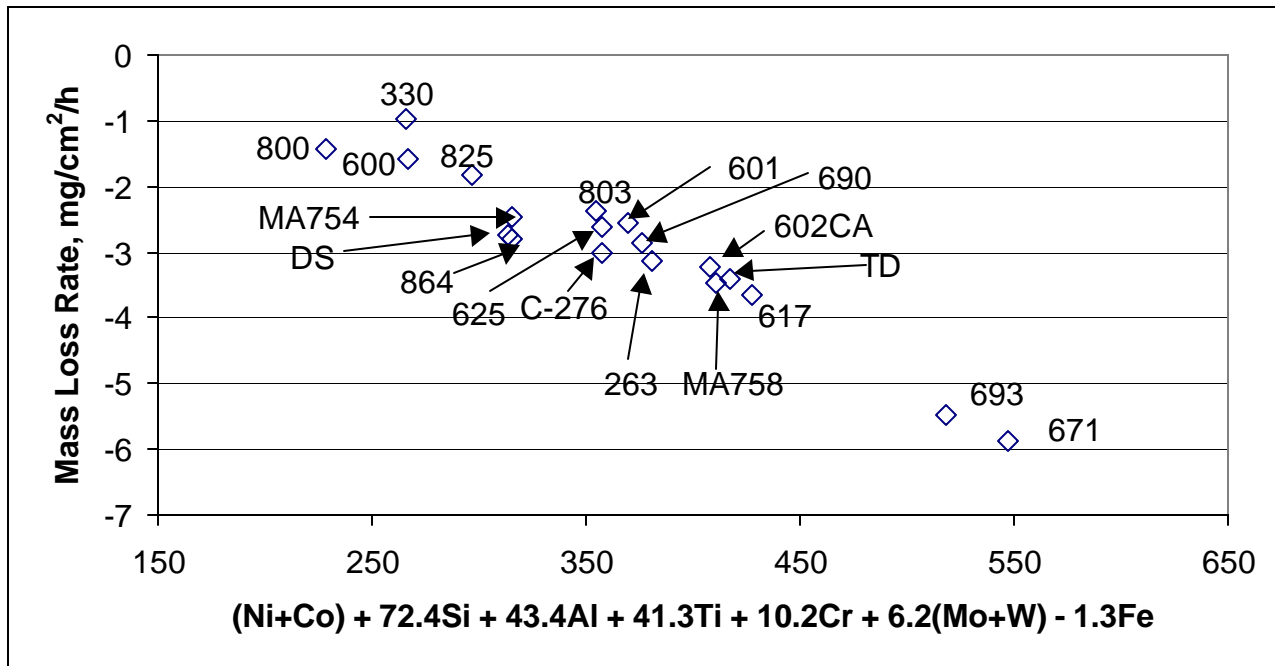


Figure 2. Results of multiple linear regression for log mass loss rate versus a summation of alloying elements in weight percent ($r^2=0.92$).

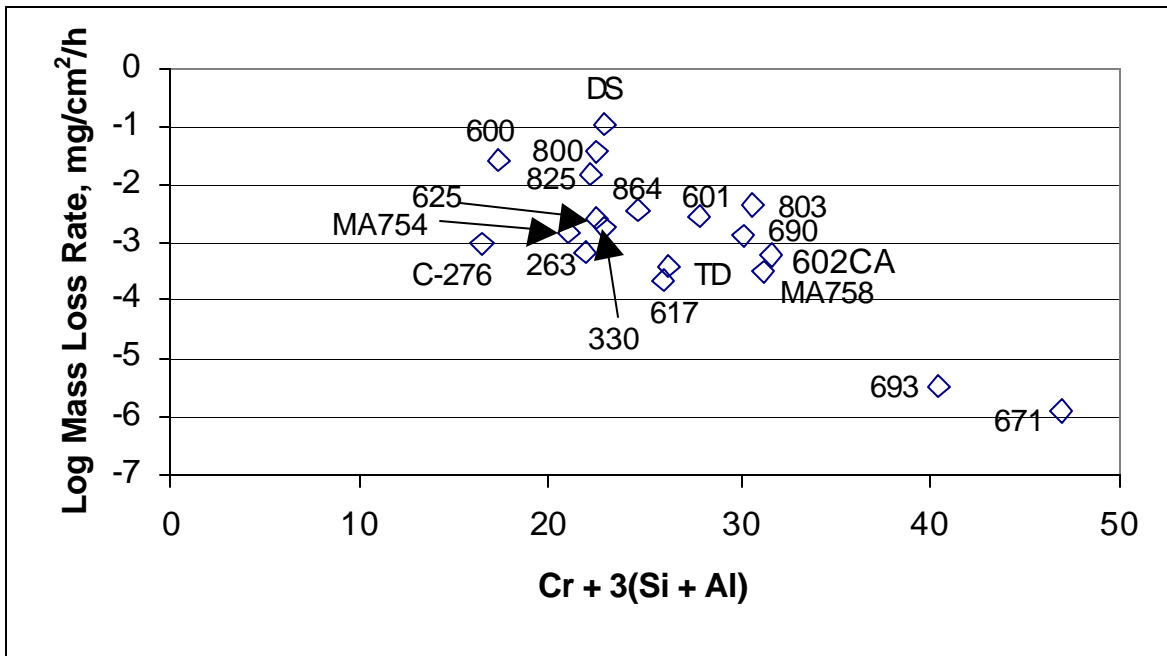


Figure 3. Results of multiple linear regression for log mass loss rate versus the 'Schillmoller chromium equivalent' summation ($r^2=0.62$).

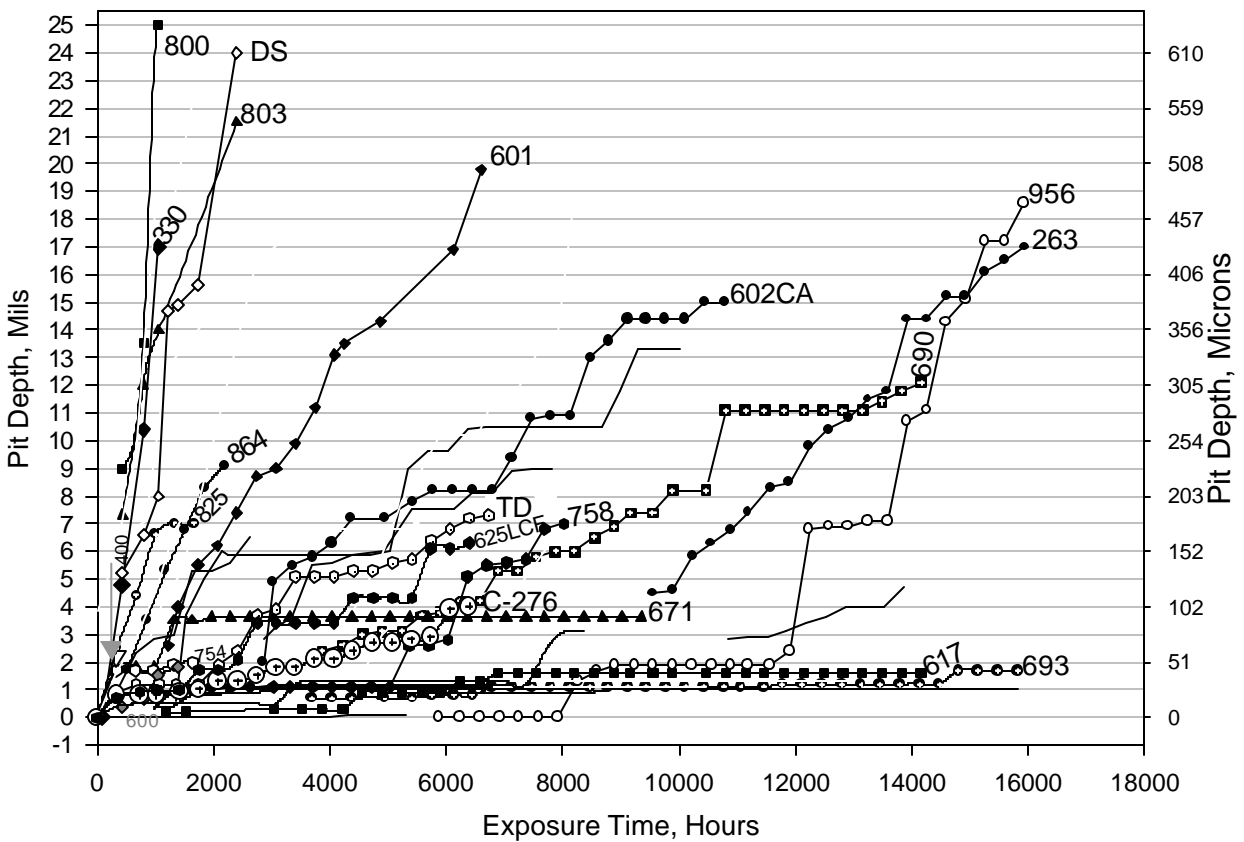


Figure 4. Maximum pit depth measurements for alloy samples exposed to CO-20% H₂ at 621°C.

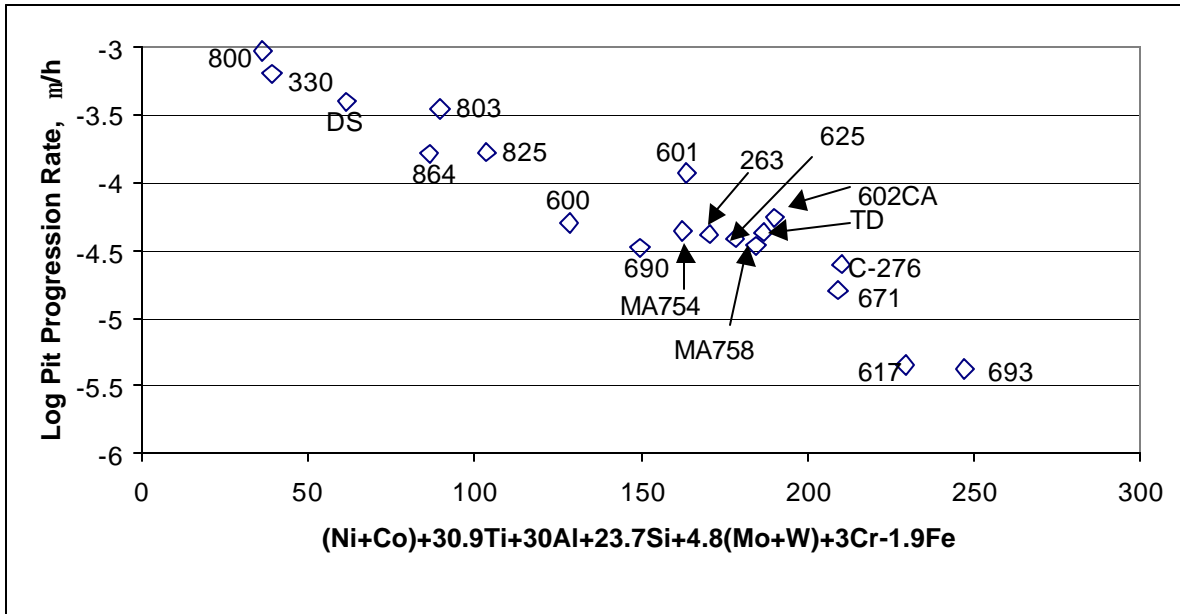


Figure 5. Results of multiple linear regression for log pit progression rate versus composition ($r^2=0.89$).

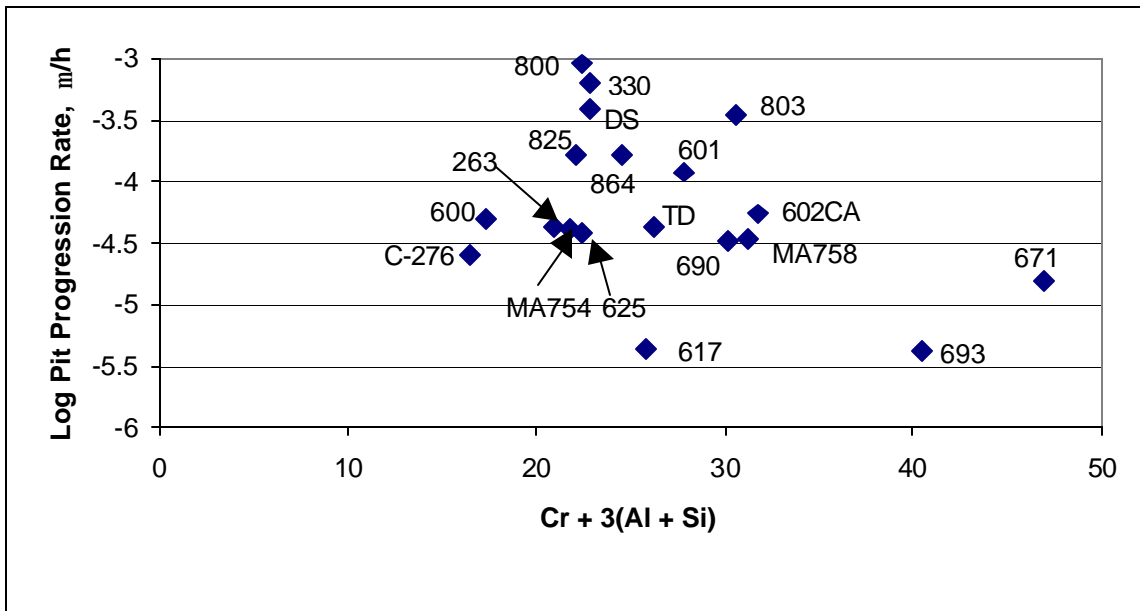


Figure 6. Results of multiple linear regression for log pit progression rate versus the 'Schillmoller chromium equivalent' summation ($r^2=0.38$).

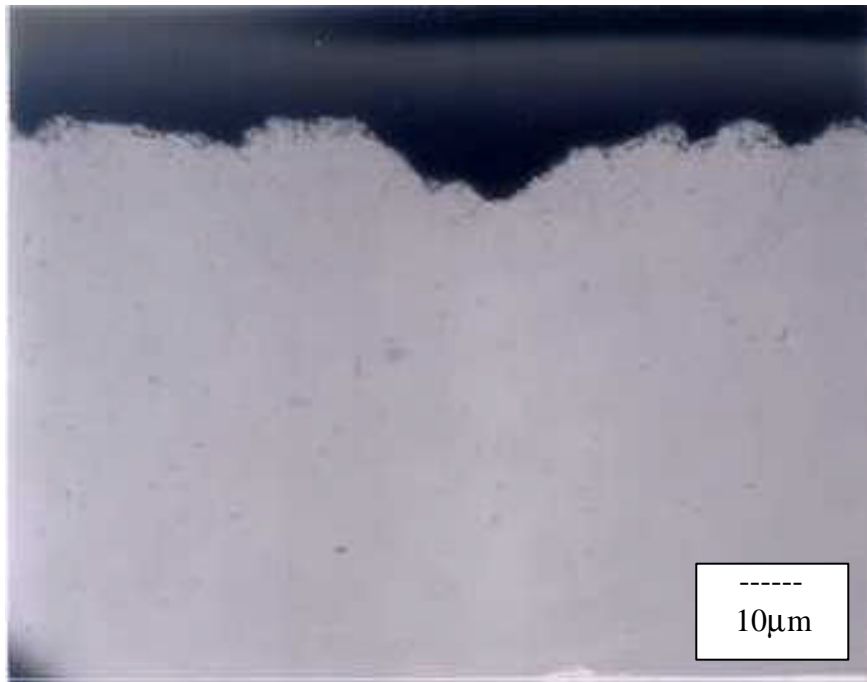


Figure 7. Photomicrograph showing the surface of alloy 693 after 15, 816 hours of exposure in CO-20% H₂ at 621°C.

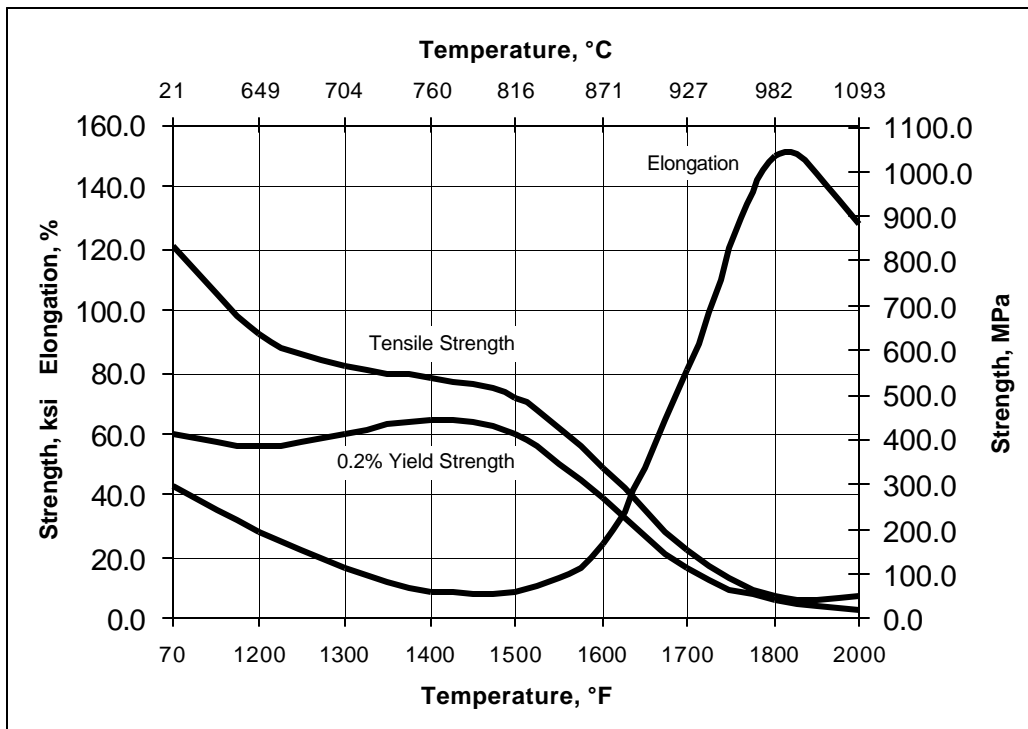


Figure 8. Tensile properties for hot-rolled and annealed alloy 693 rod.

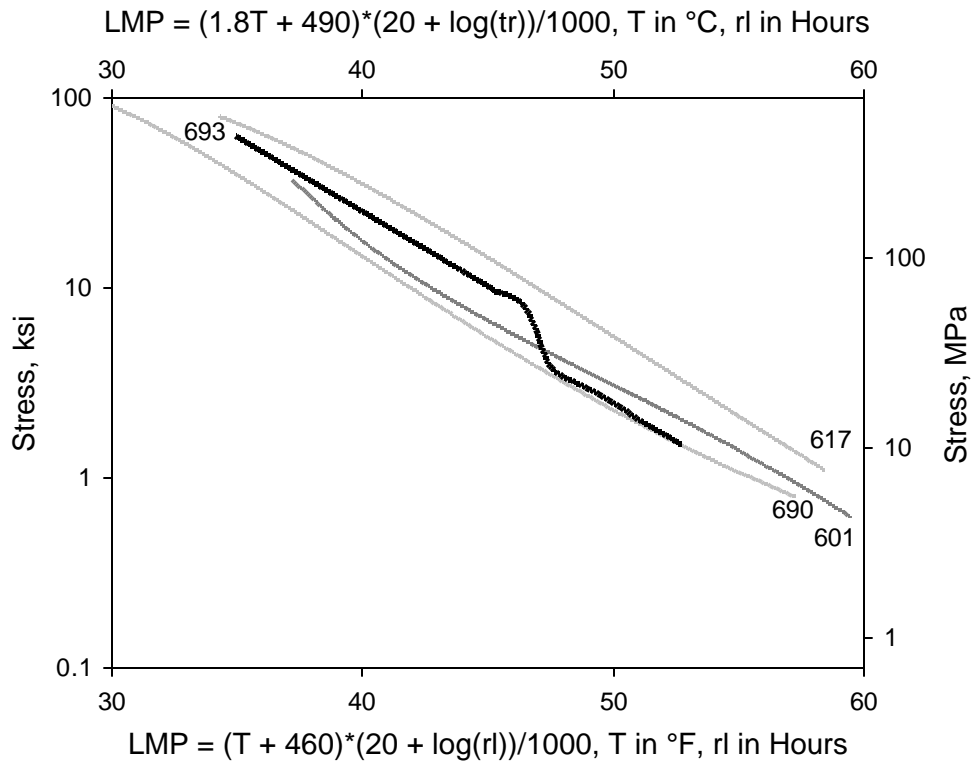


Figure 9. Creep-rupture property comparison of alloys 693, 617, 601 and 690 using the Larson-Miller parameter.

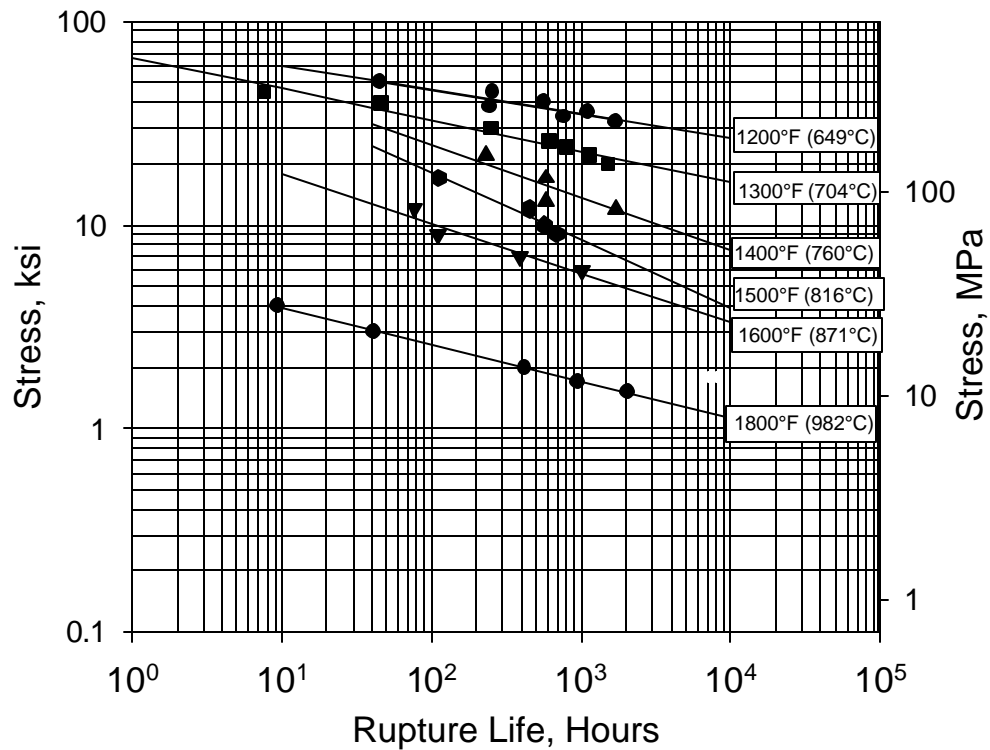


Figure 10. Creep rupture data for alloy 693.

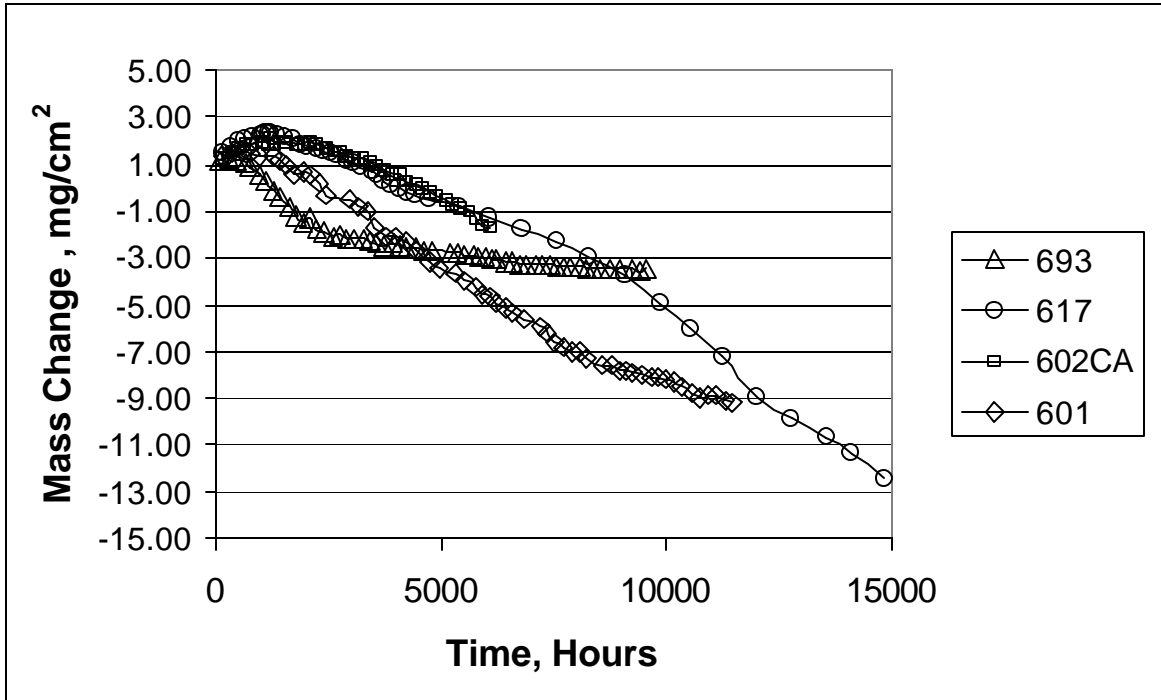


Figure 11. Mass change results for alloys 693, 617 and 601 from exposure in air + 5% water vapor at 1000°C (1832°F). Samples were cycled to room temperature weekly.

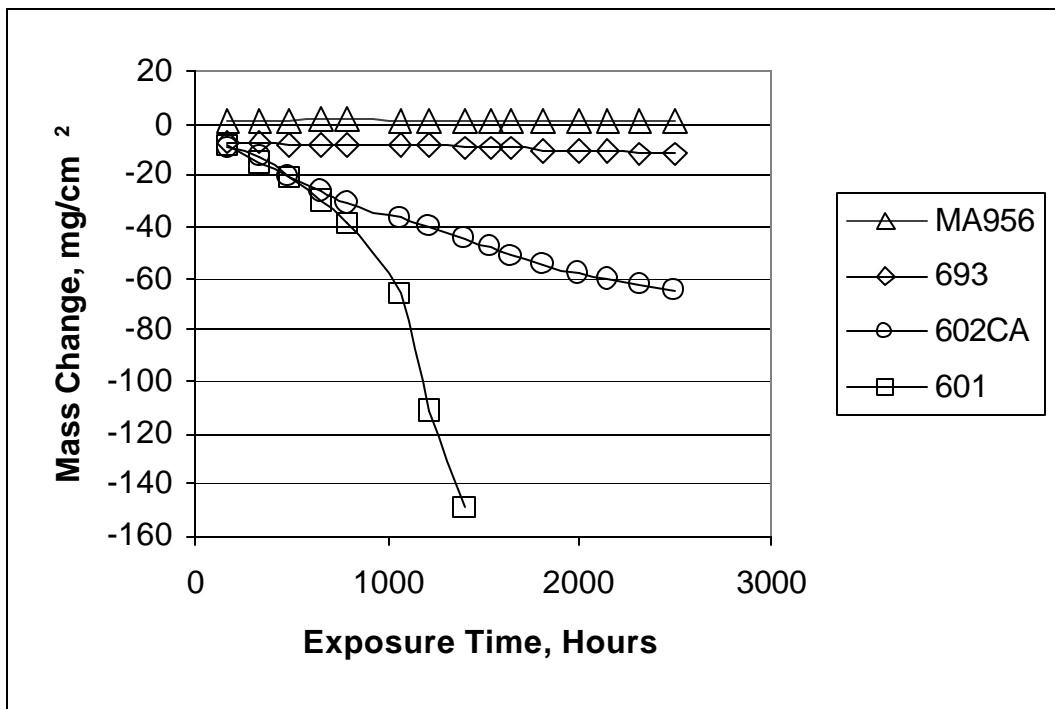


Figure 12. Mass change results for alloys 693, MA956 and 601 from exposure in air + 5% water vapor at 1200°C (2192°F). Samples were cycled to room temperature weekly.

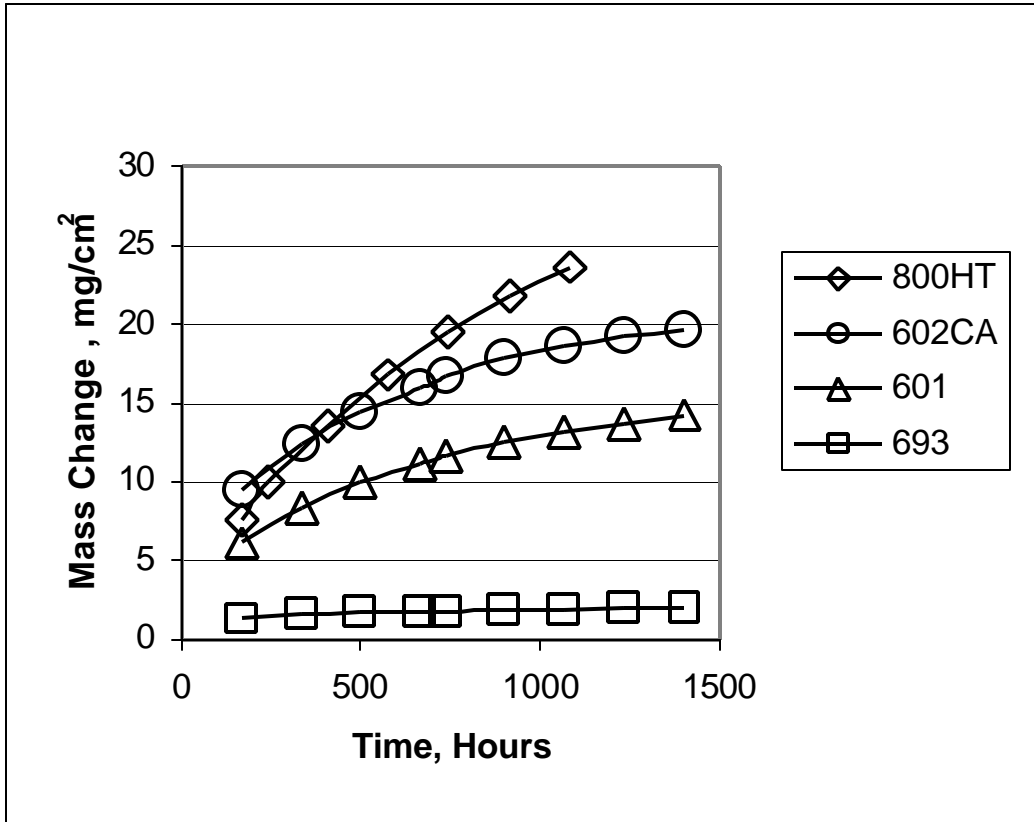


Figure 13. Mass change resulting from exposure in H_2 -5.5% CH_4 -4.5% CO_2 at 1000°C (1832°F). Samples were cycled to room temperature weekly.